ELSEVIER

Journal of Molecular Structure (Theochem) 311 (1994) 141–151

THEO CHEM

Mechanism of photochemical reaction of permanganate ion

H. Nakai, H. Nakatsuji

Department of Synthetic Chemistry, Faculty of Engineering, Kyoto University, Kyoto 606-01, Japan

(Received 19 July 1993; accepted 8 December 1993)

Abstract

The electronic mechanism of the photodecomposition reaction of MnO_4^- was investigated using an ab initio theory, taking into account electron correlation. The SAC (symmetry adapted cluster)/SAC-CI method was used to calculate the ground and excited states of the permanganate ion. It was found that to obtain reasonable descriptions of the ground and excited states of MnO_4^-, the inclusion of electron correlation is quite important. The experimental absorption spectrum of MnO_4^- was well reproduced by the present calculations. All the observed peaks were assigned to the electronic allowed transitions to the $^1T_2$ excited states. We then calculated the potential-energy curves of the ground and excited states of MnO_4^- along the reaction pathway. The resulting potential-energy curves for the ground and excited states show that the excited 1^1A_2 state plays a key role in the photochemical reaction. The energy barrier in the 1^1A_2 state determines the strong wavelength dependence of the quantum yield and the slight temperature dependence at longer wavelengths. The electronic mechanism clarified by the present ab initio study is consistent with previously reported experimental results for the photochemical decomposition of MnO_4^-.

1. Introduction

The permanganate ion MnO_4^- has been used extensively as an oxidizing agent. The electronic structures of the ground and excited states of the ion have been studied both experimentally and theoretically. Since Teltow [1] reported the visible-UV spectrum of MnO_4^- in 1938, a great deal of experimental data have been accumulated on the spectrum [1–7]. On the theoretical side, several calculations have been carried out in order to make spectral assignments [8–18]; the calculated excitation energies did not agree well with the experimental values and several different assignments were proposed.

The MnO_4^- ion in aqueous solution has been shown to be decomposed photochemically with evolution of oxygen [19–22]. The quantum yield for oxygen production was shown to depend strongly on the wavelength of the light used; namely, the shorter wavelength (311 nm) band is much more photoactive than the longer wavelength (546 nm) one. The quantum yield also depends slightly on temperature at the longer wavelengths, and not at all on the composition of the solution or on light intensity [20]. It was shown that oxygen atoms (O or O^-) are not formed by the photodecomposition reaction. Furthermore, due to the lack of an electron spin resonance (ESR) signal corresponding to the O_2^- anion, it was concluded [21] that the photodecomposition reaction proceeds through the formation of a molecular O_2 species:

$$MnO_4^- \rightarrow MnO_2^- + O_2 \quad (1)$$

SSDI 0166-1280(94)03672-8

Lee et al. [22] examined experimentally the photodecomposition process of the permanganate ion in both the presence and absence of organic substrates. Although the decomposition via Eq. (1) involves four-electron reduction of the metal, they showed an existence of a long-lived, highly oxidative intermediate. A Mn(V) peroxo complex was proposed as the intermediate. By a qualitative molecular orbital consideration, they further discussed the existence of a symmetry barrier, which prevents the intermediate from rearranging back to the tetrahedral MnO_4^- ion and gives it a long life time.

The main purpose of this study is to clarify the essential aspects of the electronic processes of the photodecomposition reaction of the permanganate ion. We first clarify the nature of the excited states involved in the electronic spectrum of the MnO_4^- ion with the use of the SAC (symmetry adapted cluster) [23]/SAC-CI [24] method, which has been shown to be very useful for studying excited and ionized states of molecules [25]. This method has also been applied to studies of the excited states of metal complexes [26–30]. Next, we examined the electronic structures of the ground and excited states of the MnO_4^- ion along the reaction pathway and attempted to clarify the electronic mechanism of the photodecomposition reaction of MnO_4^-.

2. Electronic spectrum

2.1. Computational method

To calculate the electronic spectrum, the geometry of the MnO_4^- ion was fixed at a regular tetrahedron with the experimental metal–oxygen bond length of 1.629 Å [31]. The Gaussian basis set used for manganese was the (14s8p5d)/[6s2p2d] set of Huzinaga et al. [32] augmented by two p ($\zeta_p = 0.119$, 0.039) functions [32] and one d ($\zeta_d = 0.1281$) function [33]. For oxygen we used the (9s5p)/[4s2p] set of Huzinaga and Dunning [34, 35].

The electron correlations in the ground and excited states were taken into account by using SAC/SAC-CI theory; the calculations were done using the program SAC85 [36]. The active space used in the SAC/SAC-CI calculations was [12 × 41] HF orbital space. The 12 occupied orbitals are mainly composed of the 3d atomic orbitals of manganese and the 2p atomic orbitals of oxygen. The selections of the linked and unlinked terms was performed by using the method described previously [37]. The thresholds used in the selections were 7×10^{-5} and 1×10^{-4} hartree for the ground and excited states, respectively. The dimensions of the SAC/SAC-CI calculations for the ground and excited states of MnO_4^- were from 2888 to 4529, while those of the SD-CI calculations were about 30 000. By virtue of the SAC/SAC-CI formalism, the dimensions of the calculations were small in comparison with those of the CI method of comparable accuracy.

2.2. Ground state

First we discuss the character of the valence occupied and unoccupied orbitals, which are important for the lower excited states calculated in the present study. The lowest two valence orbitals ($5t_2$ and 1e), are the bonding MOs between the 3d orbitals of manganese and the 2p orbitals of oxygen, while the unoccupied orbitals ($7t_2$ and 2e), are the antibonding MOs between them. The $5t_2$ and 2e MOs have larger amplitudes at the metal AOs than at the oxygen AOs, whilst the $7t_2$ and 1e MOs show the reverse. The excitations, $5t_2 \rightarrow 7t_2$ and $1e \rightarrow 2e$ work to weaken the covalent Mn–O bonds; the former excitation slightly increases the ionicity and the latter one reduces it. The $6t_2$ and $1t_1$ MOs are localized on the 2p orbitals of the oxygen atoms. The $6a_1$ MO is mainly composed of the 2p orbitals of oxygen and partly of the 4s orbital of manganese, and is slightly antibonding between the manganese and oxygen atoms.

The correlation energy for the ground state is −0.47605 hartree by the SAC method. The net charges on manganese were calculated to be +1.246 and +1.035 by the HF and SAC methods, respectively. Thus the Mn–O bond is calculated to be more strongly ionic by the HF method than by the SAC method. The ionic character of the Mn–O bond is relaxed by including electron correlations, as is also the case for all other metal complexes studied previously [26–30].

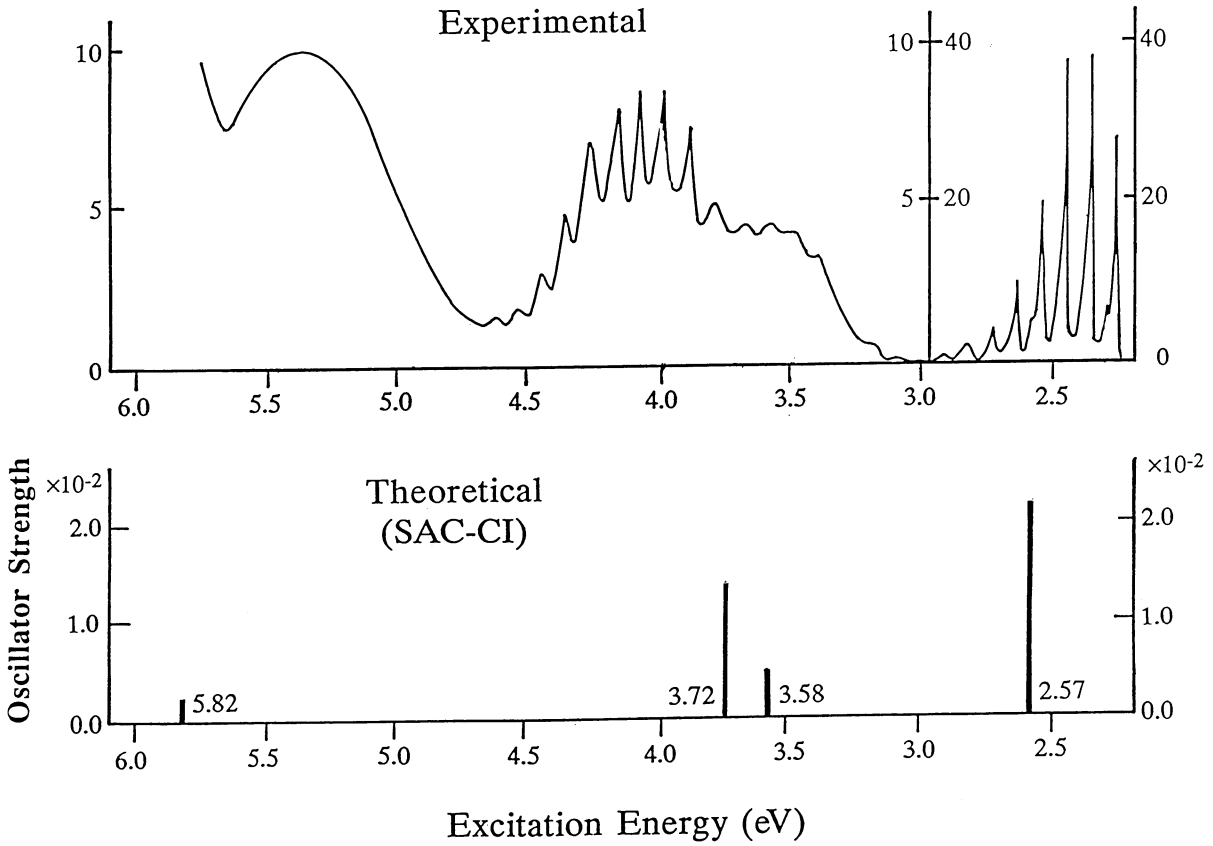

Fig. 1. Experimental and theoretical electronic excitation spectra of MnO_4^-.

2.3. Excited states

Figure 1 shows the experimental and theoretical electronic spectra of the MnO_4^- ion. In T_d symmetry, only the transitions to the $^1T_2$ states are dipole allowed. Table 1 shows a summary of the present SAC-CI results for the singlet excitation energy and oscillator strength of the excited state. We assign the observed four bands to the allowed transitions to the $^1T_2$ states. The main configurations of all the excited states shown in Table 1 are singly excited ones from either the $6t_2$, $1t_1$ or $6a_1$ MO to either the $7t_2$ or 2e MO. The $6t_2$, $1t_1$ and $6a_1$ MOs are mainly composed of the oxygen AOs, although the 4s orbital of manganese partly contributes to the $6a_1$ MO. Both the $7t_2$ and 2e MOs are delocalized all over the ion and have antibonding character between manganese and oxygen. Therefore, the transitions shown in Table 1 are all roughly characterized as electron-transfer excitations from the oxygen to the metal.

The lowest excited state was calculated to be the 1^1T_1 state ($1t_1 \rightarrow 2e$), the excitation energy being 2.18 eV. As the transition to the 1^1T_1 state is dipole forbidden, the corresponding transition peak is not seen in the experimental spectrum of Fig. 1. In the lithium and barium salts $LiMnO_4 \cdot 3H_2O$ and $Ba(MnO_4)_2 \cdot 3H_2O$, the corresponding transitions are observed at 1.71 and 1.77 eV because of the C_{3v} and C_3 symmetries, respectively.

The first strong band observed at 2.27 eV is assigned to the allowed transition to the 1^1T_2 state ($1t_1 \rightarrow 2e$), the excitation energy of which is 2.57 eV. Our assignment for the first band is the same as those proposed from ΔSCF [15] and SD-CI [18] calculations. The corresponding transition was calculated for the 3^1T_2 or 2^1T_2 state by using the SE-CI method [12, 13]. We show later that the

Table 1
Summary of the ground and excited states of MnO_4^-

State	SAC/SAC-CI			Experimental	
	Main configuration	Excitation energy[a]	Oscillator strength	Excitation energy	Oscillator strength[b]
XA_1	HF	0.00	–	–	–
$1T_1$	$1t_1 \rightarrow 2e$	2.18	Forbidden	(1.71–1.77)	
$1T_2$	$1t_1 \rightarrow 2e$	2.57 (+0.30)	0.0202	2.27	S
$2T_1$	$6t_2 \rightarrow 2e$	3.33	Forbidden		
$1E$	$1t_1 \rightarrow 7t_2$	3.41	Forbidden		
$2E$	$6a_1 \rightarrow 2e$	3.54	Forbidden		
$2T_2$	$1t_1 \rightarrow 7t_2$	3.58 (+0.11)	0.0045	3.47	W
$3T_2$	$6t_2 \rightarrow 2e$	3.72 (−0.27)	0.0136	3.99	S
$3T_1$	$1t_1 \rightarrow 7t_2$	4.12	Forbidden		
$1A_2$	$1t_1 \rightarrow 7t_2$	4.46	Forbidden		
$4T_1$	$6t_2 \rightarrow 7t_2$	5.30	Forbidden		
$2A_1$	$6t_2 \rightarrow 7t_2$	5.41	Forbidden		
$3E$	$6t_2 \rightarrow 7t_2$	5.47	Forbidden		
$4T_2$	$6t_2 \rightarrow 7t_2$ $6a_1 \rightarrow 7t_2$	5.82 (+0.37)	0.0022	5.45	S

[a]Values in parentheses show the difference from the experimental values.
[b]S, strong; W, weak.

SE-CI method is totally unreliable for this molecule. The excitation energy calculated using the ΔSCF procedure is about 1.2 eV lower than the experimental value, which shows that the correlation error in the ground state is much larger than that in the excited state.

The second and third bands are assigned to the transitions to the 2^1T_2 ($1t_1 \rightarrow 7t_2$) and 3^1T_2 ($6t_2 \rightarrow 2e$) states, respectively. The calculated excitation energies are 3.58 and 3.72 eV, respectively. The calculated oscillator strength is smaller for the former than for the latter, which agrees with the order of the strengths of the experimental peaks.

The fourth peak observed at 5.45 eV is assigned by the present calculation to the transition to the 4^1T_2 state, which is calculated to lie 5.82 eV above the ground state. The discrepancy from the experimental value is 0.37 eV. The main configurations are the mixtures of $6a_1 \rightarrow 7t_2$ and $6t_2 \rightarrow 7t_2$. The calculated oscillator strength is 2.2×10^{-3}; this is a relatively small value, although the intensity of the observed peak is strong. We think that the intensity of this peak does not originate from this transition only, because it is located at the shoulder of the higher energy band.

2.4. Electron correlation effects

In the present study we used three different sizes of active unoccupied space for the SAC/SAC-CI calculations: 19, 31, and 41 unoccupied orbitals. The calculation with the [12 × 41] active space was the most reliable one. The SE-CI calculations were also carried out within the [12 × 41] active space. The SE-CI calculation gave the $1t_1 \rightarrow 7t_2$ state as the lowest and the $1t_1 \rightarrow 2e$ state as the third allowed state at 4.75 eV above the ground state. This result is similar to the previously reported SE-CI results [12, 13]. However, by the SAC/SAC-CI method, the lowest transition is always to the $1t_1 \rightarrow 2e$ state. As the size of the active unoccupied space increases, the excitation energy decreases and comes closer to the experimental value. The differences between the SE-CI and SAC/SAC-CI energies calculated within the [12 × 41] active space are −2.48 and +0.61 eV to the $1t_1 \rightarrow 2e$ and $1t_1 \rightarrow 7t_2$ states, respectively. We therefore conclude that for a reasonable and even qualitative assignment of the excitation spectrum of MnO_4^-, it is quite important to include sufficiently large electron

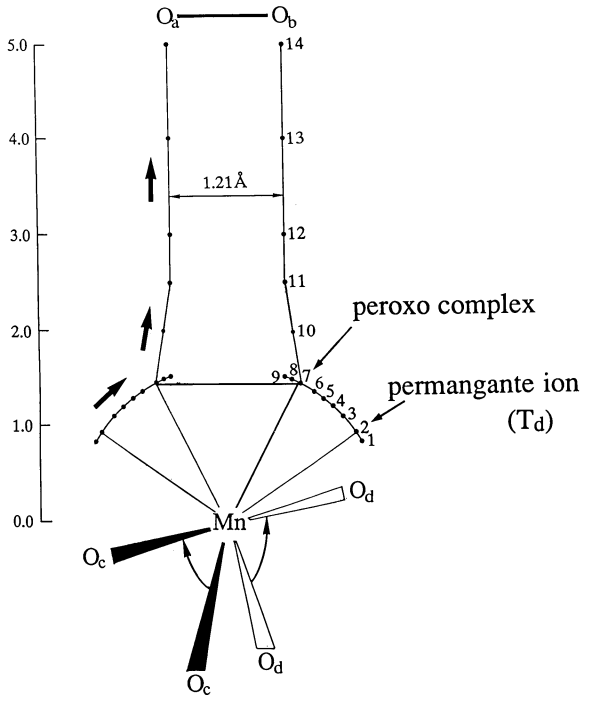

Fig. 2. Reaction pathway for the decomposition of the permanganate ion into MnO_2^- and O_2.

correlations within a large active space. This is necessary for sufficient relaxation of the valence electrons.

3. Photochemical decomposition reaction

3.1. Reaction pathway

It has been clarified by experimental studies that in the photodecomposition reaction of the MnO_4^- ion only molecular oxygen is generated, and no atomic oxygen is involved. We therefore assume the reaction pathway as shown in Fig. 2. In this reaction path, the O_a and O_b atoms mainly move and dissociate from the O_c-Mn-O_d system, whilst the C_{2v} symmetry is maintained. The O_a and O_b atoms are located in the xz plane and the O_c and O_d atoms in the yz plane. Over the positions 1 to 9, the O_a-O_b distance was changed from 2.80 to 1.21Å with the $Mn-O_{c(d)}$ distances kept fixed at 1.629 Å, the equilibrium distance of the MnO_4^- ion [31]. Over positions 7 to 14 the distance between the manganese atom and the centre of O_2 (Fig. 2) was changed from 1.48 to 5.00 Å. The geometry optimizations of the ground state by the HF method indicate that the O_c-Mn-O_d angle and the O_c-O_d distance do not change much over positions 1 to 9, while the O_c-Mn-O_d angle changes from a tetrahedral (T_d) angle to linear between positions 7 and 14. Therefore, the $Mn-O_c$ and $Mn-O_d$ distances were fixed at 1.629 Å and the O_c-Mn-O_d angle was fixed at the T_d angle for positions 1 to 9. The optimized O_a-O_b distance at position 10 is 1.39 Å, while for positions 11 to 14 it is close to 1.21 Å, the equilibrium distance of a free O_2 molecule [38]. We examined the reactions of the excited states using the same pathway as the ground state.

3.2. Wavefunctions

The effective core potential was used for the neon core of the manganese atom and the Gaussian (5s5p5d)/[4s3p2d] set was used for the valence electrons [39]. For oxygen we used the (9s5p)/[4s2p] set of Huzinaga and Dunning [34, 35] augmented by the diffuse s,p functions of $\zeta = 0.059$ as anion bases [40].

The potential-energy curve of the singlet ground state was calculated using the HF and SAC methods, and those of the singlet excited states was calculated by using the SAC-CI method. The active space in the SAC/SAC-CI calculations is [12 × 29] HF orbital space. The thresholds used in the selections were 5×10^{-5} and 1×10^{-4} hartree for the ground and excited states, respectively. The potential-energy curves of the singlet, triplet, and quintet states were calculated using the CI method at positions 7 to 14. In the CI calculations, four electron excitations were considered in the active space of [12 × 2]; these correspond to the full excitations.

3.3. Separated system

First, we studied the energy and the electronic structures of the separated system, $O_2 + MnO_2^-$ or $O_2^- + MnO_2$. We performed the SAC/SAC-CI calculations for the free MnO_2 and MnO_2^- mol-

Table 2
Total energy of the MnO_2 species

Structure	State	Total energy (hartree)	ΔE[a] (kcal mol^{-1})
Bent	$^1A_1$ (anion)	−252.813201	0.00
	$^3B_1$ (anion)	−252.828420	−9.54
	$^2A_1$ (neutral)	−252.739623	+46.14
Linear	$^1\Sigma_g^+$ (anion)	−252.805555	+4.79
	$^1\Delta_g$ (anion)	−252.832735	−12.25
	$^3\Delta_g$ (anion)	−252.881897	−43.08
	$^2\Delta_g$ (neutral)	−252.740221	+45.76

[a]Energy difference from the $^1A_1$ state of the bent MnO_2 system.

Table 3
Total energy of the O_2 species

Species	State	Total energy (hartree)	ΔE[a] (kcal mol^{-1})
O_2	$^3\Sigma_g^-$	−149.599001	0.00
	$^1\Delta_g$	−149.562924[b]	+22.62[c]
O_2^-	$^2\Pi_g$	−149.615171[b]	−10.14[d]

[a]Energy difference from the $^3\Sigma_g^-$ state of the free O_2 molecule.
[b]Estimated from the experimental excitation energy and electron affinity.
[c]Ref. 38.
[d]Ref. 41.

ecules. The active space used in the calculations was the [8 × 19] orbital space, and for the configuration selection of the linked and unlinked terms the same thresholds as used in the SAC/SAC-CI calculations on MnO_4^- were adopted. The O–Mn–O angle was changed from 90° to 180° with the Mn–O distance kept fixed at 1.629 Å.

The calculated total energies for the lower states of the MnO_2 species are shown in Table 2. The most stable geometries of both the MnO_2 and the MnO_2^- molecules are the linear systems, and their ground states are $^2\Delta_g$ and $^3\Delta_g$, respectively. The ground state of MnO_2^- is much more stable than that of MnO_2. The open-shell $^1\Delta_g$ and $^3\Delta_g$ states of MnO_2^- have formal $3d^9 4s^1$ configurations of manganese and the closed-shell $^1\Sigma_g^+$ state has a $3d^{10}4s^0$ configuration.

We then estimated the total energy of the free O_2 molecule. As the SAC/SAC-CI method using the SAC85 program does not describe well the ground $^3\Sigma_g^-$ state of O_2, we calculated the ground $^2\Pi$ state of the O_2^- anion as an ionized state of O_2^{2-} by using the SAC/SAC-CI method and the total energy of O_2 was estimated by using the experimental electron affinity (EA) of O_2 (10.14 kcal mol^{-1} [41]). The O–O distance of 1.35 Å [38], which is the equilibrium distance of O_2^-, was used for the SAC/SAC-CI calculations, because the EA of O_2 is observed adiabatically. The active space used in the calculations was the [5 × 9] orbital space. The total energy of the $^1\Delta_g$ state of O_2 was estimated using the experimental excitation energy from $^3\Sigma_g^-$ to $^1\Delta_g$ [38]. The total energies for the O_2 species thus calculated are summarized in Table 3.

3.4. Potential-energy curves

Next, we investigated the electronic structure and the potential-energy curve of the ground state of the MnO_4^- ion along the reaction pathway. Figure 3 shows the potential-energy curves calculated using the HF, CI and SAC-CI methods.

In the bending process from positions 1 to 9, where only the O_a–Mn–O_b angle changes, the ground state of MnO_4^- is in the closed-shell $^1A_1$ state. There are two potential minima on both the HF and the SAC curves, one at position 2 and the other at the O_a–Mn–O_b angle of about 55°. The former minimum is situated at the equilibrium structure of the permanganate ion. However, in the latter minimum the O_a–O_b distance is about 1.5 Å. In this state, the parallel π^* orbital of O_2 interacts attractively with the d_{xz} orbital of manganese, while the perpendicular π^* orbital is localized at the oxygen molecule. As these π^* orbitals of O_2 are formally occupied by four electrons, this state corresponds to a peroxo complex.

The HF calculation shows that the peroxo complex is more stable than the T_d permanganate complex, which is not consistent with the experimental equilibrium geometry of MnO_4^-. However, the SAC calculation indicates that the permanganate structure is the more stable one. This result clearly shows that the inclusion of electron correlation is quite important even for a qualitative description of the equilibrium geometry of MnO_4^-.

In the peroxo complex, the σ orbital of O_2, which has a_1 symmetry, is doubly occupied and has a slightly antibonding interaction between MnO_2

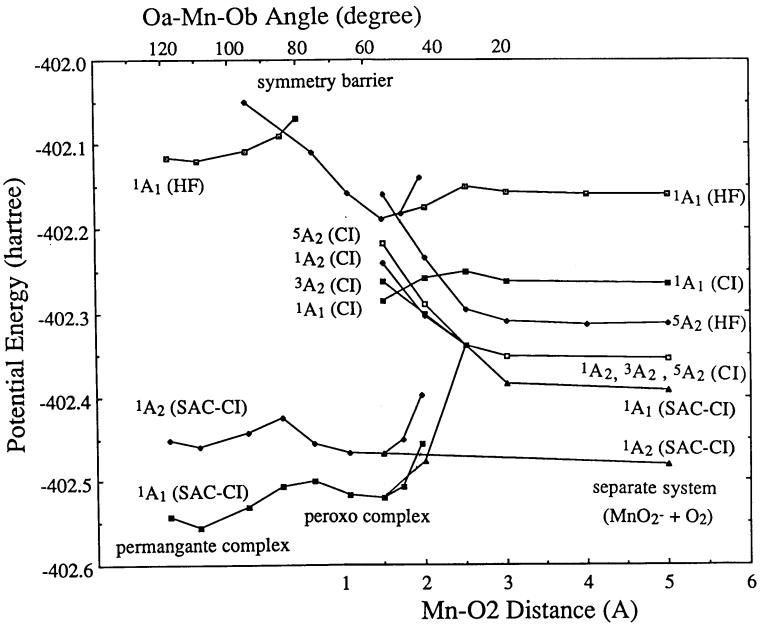

Fig. 3. Potential-energy curves of the low-lying states of MnO_4^- calculated using the HF, CI and SAC-CI methods.

and O_2, while the σ^* orbital of O_2 with symmetry b_1 is unoccupied. In the transformation process between the permanganate and peroxo complexes, a two-electron transition occurs between the a_1 and b_1 orbitals. The two-electron transition contributes to the O–O bond formation and partially to the Mn–O bond breaking. The potential barrier between them is due to the avoided crossing of the two $^1A_1$ states and corresponds to the symmetry barrier pointed out by Lee et al. [22]. As the HF method cannot describe this avoided crossing well, the potential-energy curve from the HF calculations has a cusp at the barrier; the SAC method can describe this avoided crossing and gives a reasonable potential-energy curve. The barrier heights calculated using the SAC method are 13 and 34 kcal mol^{-1} for the conversions to the permanganate and the peroxo complexes, respectively.

In the dissociation process from positions 7 to 14, where the O_a–O_b molecule separates from the MnO_2 system, the ground state changes from the closed-shell $^1A_1$ state to the open-shell A_2 state. All the $^1A_1$ curves obtained from the HF, Cl and SAC-CI calculations have a barrier at the Mn–O_2 distance of 2.5 Å. The energy barrier obtained from the SAC-CI calculations is much higher than that from the HF ones, which shows that the electron correlations of the peroxo complex are greater than those of the barrier. They are also greater than those of the separated system.

However, all the A_2 curves are repulsive. The CI results show that the singlet, triplet and quintet A_2 curves overlap at Mn–O_2 distances of 2.5–5.0 Å. This state corresponds to the ground $^3\Delta_g$ state of MnO_2^- plus the ground $^3\Sigma_g^-$ state of O_2. As the SAC/SAC-CI method using SAC85 program does not describe well this ground state of the separated system, $MnO_2^- + O_2$, we used the estimated energy (Tables 2 and 3).

Figure 4 shows the potential-energy curves of the ground and excited states in the bending process. The potential-energy curves of the excited states are rather crowded and close to each other, while there is a large energy gap of 40 ~ 60 kcal mol^{-1} between the ground and the lowest excited states. As the internal conversion between the states with similar energy levels can easily occur, the vertically excited state at the T_d structure would be relaxed to the 1^1T_1–1^1A_2 state after internal conversions among the excited states. This process is certainly realistic with regard to the Kasha rule, which means

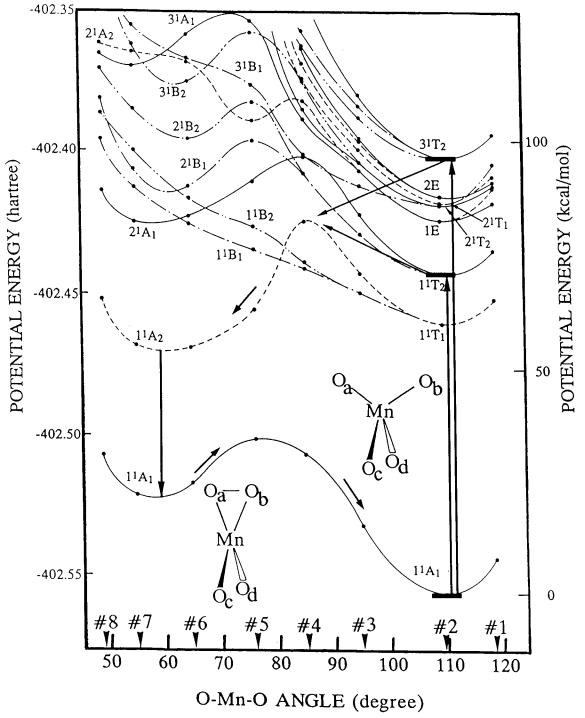

Fig. 4. Potential-energy curves of the ground and excited states of MnO_4^- in the bending process calculated using the SAC-CI method.

that the photochemical reactions proceed along the lowest excited states. The 1^1A_2 state is connected with the 1^1T_1 state, when the symmetry of the ion changes from T_d to C_2v. Note that in the 1^1A_2 state the potential energy at the peroxo structure is lower than that at the permanganate one, while in the other states the former energies are higher. This shows that when the excited ion is relaxed to the 1^1A_2 state it is liable to change its geometry from the T_d structure to the peroxo one and to separate the system further, while there is a potential barrier at position 4. The potential energy of the 1^1T_2 state is lower than the potential barrier of the 1^1A_2 state, while that of the 3^1T_2 state is higher.

3.5. *Mechanism of photodecomposition reaction*

Figure 5 shows the energy diagram for the photochemical reaction of MnO_4^- calculated in the present study, and Scheme 1 shows the proposed reaction. With reference to the energy diagram and the scheme, the mechanism of the photochemical reaction can be explained as follows.

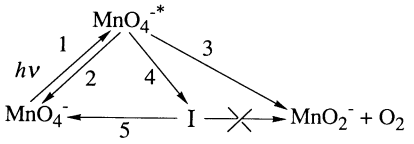

Scheme 1.

Absorption of light at the T_d structure is the first step in the photochemical reaction of MnO_4^- (1 in Fig. 5 and Scheme 1). The absorption of light of wavelengths 546 and 311 nm is assigned to the dipole-allowed transitions to the 1^1T_2 and the 3^1T_2 states, respectively. The excitation to the 2^1T_2 state is not observed in the photodecomposition experiments, probably because of the smaller transition probability for this state than for the 1^1T_2 and 3^1T_2 states.

The quenching of the photo-excited ion occurs at the T_d structure and decreases the quantum yield of the photochemical reaction (2 in Fig. 5).

The photo-excited MnO_4^- then relaxes to the lowest excited $1^1T_1-1^1A_2$ state, the geometry changing from the T_d structure to the peroxo one, and then to the separated system. When this internal conversion starts from the 1^1T_2 state, the process must go over the energy barrier, and thus will depend on the temperature despite the fact that it is a photochemical process. However, when the ion is converted from the 3^1T_2 state it has sufficient energy to go over the barrier. This difference seems to be the reason for the wavelength dependence of the quantum yield; that is, the quantum yield for the shorter wavelength is much larger than that for the longer one. This process is shown by 3 in Fig. 5.

As the potential-energy curves of the 1^1A_1 and 1^1A_2 states cross in the dissociation process, the internal conversion from the 1^1A_2 to 1^1A_1 states occurs there. This conversion leads to the ground state of the peroxo complex, which is the intermediate proposed by Lee et al. [22]. This process is shown by 4 in Fig. 5.

The intermediate can return back to the permanganate ion. While the barrier to this process is comparatively small, it is the symmetry barrier as mentioned before. This process, therefore,

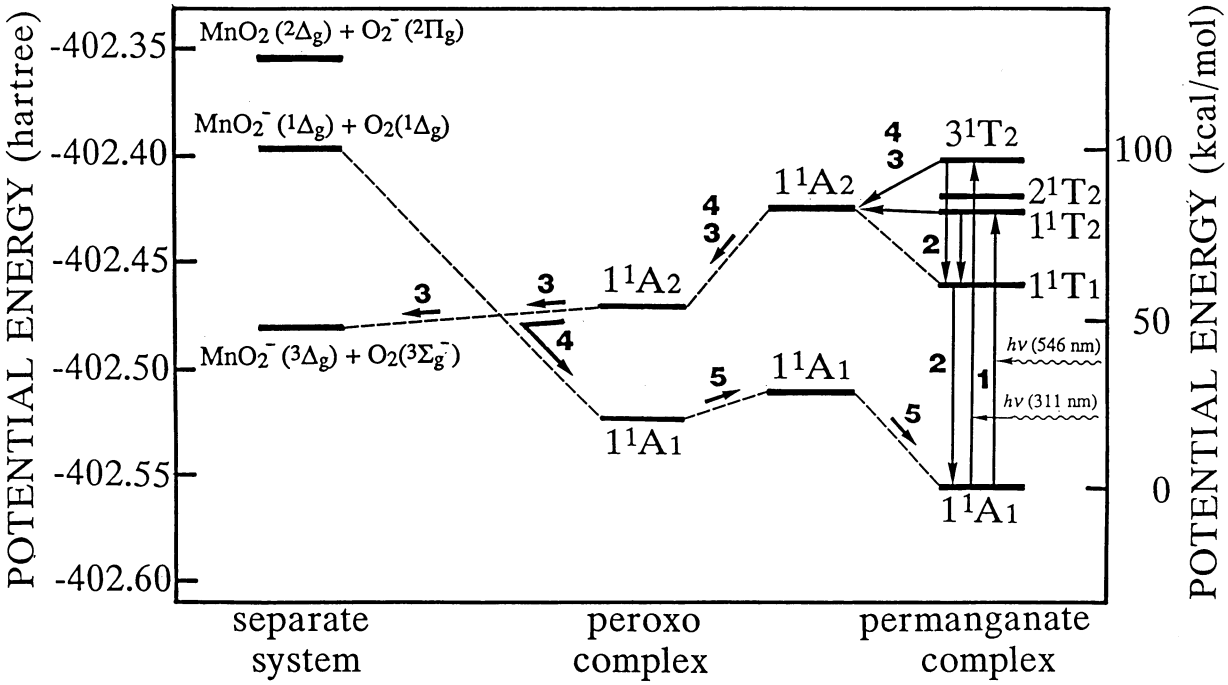

Fig. 5. Energy diagram of the photochemical reaction of MnO_4^-.

is Woodward–Hoffmann forbidden and the intermediate would have a long life time, which is observed experimentally. This process is shown by 5 in Fig. 5.

On the basis of experimental observations, Lee et al. [22] proposed a scheme for the photochemical reaction of MnO_4^- which involves the formation of the intermediate. The scheme agrees with the present mechanism except for the decomposition process (3 in Fig. 5). They proposed that the decomposition into $MnO_2^- + O_2$ occurs from the intermediate, while the present study shows that it occurs directly from the photo-excited ion.

4. Concluding remarks

In the present study, we have tried to clarify the electronic mechanism of the photo-decomposition reaction of MnO_4^- by using ab initio theories and including electron correlation. The SAC/SC-CI method was used to calculate the potential-energy curves for the ground and excited states of the permanganate ion along the reaction pathway.

We used the SAC/SAC-CI method to calculate the ground and excited states of MnO_4^-. The theoretical excitation spectrum calculated using the SAC-CI method reproduces the experimental spectrum well. The observed four peaks are assigned as being due to the dipole-allowed transitions to the $^1T_2$ state. We propose the present SAC-CI assignment as a reliable one as a sufficient amount of electron correlation was included, which differs from previous studies (Fig. 2).

In addition, we clarified the electronic mechanism of the photochemical decomposition reaction of MnO_4^-. Our calculations are consistent with the previously reported experimental results. In this reaction, the 1^1A_2 state plays a key role. Along the potential-energy curve of the 1^1A_2 state the photo-excited ion leads to the separated system. The energy barrier in the 1^1A_2 curve determines the strong wavelength dependence of the quantum yield and the slight temperature

dependence when the longer wavelength light was used.

The details of the spectrum of MnO_4^- are discussed in Ref. 42, and the details of the study on the photochemical decomposition of MnO_4^- will be published in the near future [43].

Acknowledgments

The calculations were carried out using the computers at the Data Processing Center of Kyoto University and at the Institute for Molecular Science. This study was partially supported by a Grant-in-Aid for Scientific Research from the Japanese Ministry of Education, Science, and Culture.

References

[1] J. Teltow, Z. Phys. Chem., Abt. B, 40 (1938) 397; 43 (1939) 198.
[2] A. Carrington and M.C.R. Symons, J. Chem. Soc., (1956) 3373.
[3] L. Holt and C.J. Ballhausen, Theor. Chim. Acta, 7 (1967) 313.
[4] P. Day, L. DiSipio and L. Oleari, Chem. Phys. Lett., 5 (1970) 533.
[5] L.W. Johnson and S.P. McGlynn, J. Chem. Phys., 55 (1971) 2985.
[6] L.W. Johnson and S.P. McGlynn, Chem. Phys. Lett., 10 (1971) 595.
[7] L.W. Johnson, E. Hughes and S.P. McGlynn, J. Chem. Phys., 55 (1971) 4476.
[8] M. Wolfsberg and L. Helmholz, J. Chem. Phys., 20 (1952) 837.
[9] K.H. Johnson and F.C. Smith, Jr., Chem. Phys. Lett., 10 (1971) 219.
[10] T. Sakaki and H. Adchi, J. Electron Spectrosc. Relat. Phenom., 19 (1980) 261.
[11] A. Golebiewski and M. Witko, Acta. Phys. Pol. A, 57 (1980) 585.
[12] I.H. Hillier and V.R. Saunders, Proc. R. Soc. London, Ser. A, 320 (1970) 161.
[13] I.H. Hillier and V.R. Saunders, Chem. Phys. Lett., 9 (1971) 219.
[14] P.D. Dacre and M. Elder, Chem. Phys. Lett., 11 (1971) 377.
[15] H. Johansen, Chem. Phys. Lett., 17 (1972) 569.
[16] T. Ziegler, A. Rauk and E.J. Baerends, Chem. Phys., 16 (1976) 209.
[17] H. Hsu, C. Peterson and R.M. Pitzer, J. Chem. Phys., 64 (1976) 791.
[18] H. Johansen and S. Retrup, Chem. Phys., 74 (1983) 77. H. Johansen, Mol. Phys., 49 (1983) 1209.
[19] J.H. Mathews and L.H. Dewey, J. Phys. Chem., 17 (1913) 211.
[20] G. Zimmerman, J. Chem. Phys., 23 (1955) 825.
[21] U. Kläning and M.C.R. Symons, J. Chem. Soc., (1959) 3269.
[22] D.G. Lee, C.R. Moylan, T. Hayashi and J.I. Brauman, J. Am. Chem. Soc., 109 (1987) 3003.
[23] H. Nakatsuji and K. Hirao, J. Chem. Phys., 68 (1978) 2035.
[24] H. Nakatsuji, Chem. Phys. Lett., 59 (1978) 362; 67 (1979) 329, 334.
[25] H. Nakatsuji, Acta. Chim. Hung., 129 (1992) 719.
[26] H. Nakatsuji and S. Saito, Int. J. Quantum Chem., 39 (1991) 93.
[27] H. Nakatsuji and S. Saito, J. Chem. Phys., 93 (1990) 1865.
[28] H. Nakatsuji, M. Ehara, M.H. Palmer and M.F. Guest, J. Chem. Phys., 87 (1992) 2561.
[29] K. Yasuda and H. Nakatsuji, J. Chem. Phys., 99 (1993) 1945.
[30] S. Jitsuhiro, H. Nakai, M. Hada and H. Nakatsuji, J. Chem. Phys., in press.
[31] G.J. Palenik, Inorg. Chem., 6 (1967) 503.
[32] S. Huzinaga, J. Andzelm, M. Klobukowski, E. Radzio-Andzelm, Y. Sakai and H. Tatewaki, Gaussian Basis Sets for Molecular Calculations, Elsevier, New York, 1984.
[33] A.K. Rappe, T.A. Smedley and W.A. Goddar III, J. Phys. Chem., 85 (1981) 2607.
[34] S. Huzinaga, J. Chem. Phys., 42 (1965) 1293.
[35] T.H. Dunning, Jr., J. Chem. Phys., 53 (1970) 2823.
[36] H. Nakatsuji, Program System for SAC and SAC-CI calculations, Program Library No. 146 (Y4/SAC), Data Processing Center of Kyoto University, 1985. Program Library SAC85, No. 1396, Computer Center of the Institute for Molecular Science, 1981.
[37] H. Nakatsuji, Chem. Phys., 75 (1983) 425.
[38] K.P. Huber and G. Herzberg, Molecular Spectra and Molecular Structure. IV Constants of Diatomic Molecules, Van Nostrand Reinhold, New York, 1979.
[39] P.J. Hay and W.R. Wadt, J. Chem. Phys., 82 (1985) 299.
[40] T.H. Dunning, Jr., and P.J. Hay, in H.F. Schaeffer III

(Ed.), Modern Theoretical Chemistry, Vol. 3, Plenum, New York, 1977.
[41] R.J. Celotta, R.A. Bennett, J.L. Hall, M.W. Siegel and J. Levine, Phys. Rev. A, 6 (1972) 607.
[42] H. Nakai, Y. Ohmori and H. Nakatsuji, J. Chem. Phys., 95 (1991) 8287.
[43] H. Nakai, Y. Ohmori and H. Nakatsuji, J. Am. Chem. Soc., submitted for publication.